Nuclear factor-κB bioluminescence imaging-guided transcriptomic analysis for the assessment of host–biomaterial interaction *in vivo*

Chien-Yun Hsiang[a], Yueh-Sheng Chen[b] and Tin-Yun Ho[c, d, ,]

[a] Department of Microbiology, China Medical University, Taichung 40402, Taiwan

[b] Biomaterials Laboratory, Graduate Institute of Chinese Medical Science, China Medical University, Taichung 40402, Taiwan

[c] Molecular Biology Laboratory, Graduate Institute of Chinese Medical Science, China Medical University, 91 Hsueh-Shih Road, Taichung 40402, Taiwan

[d] Department of Nuclear Medicine, China Medical University Hospital, Taichung 40447, Taiwan

Abstract

Establishment of a comprehensive platform for the assessment of host–biomaterial interaction *in vivo* is an important issue. Nuclear factor-κB (NF-κB) is an inducible transcription factor that is activated by numerous stimuli. Therefore, NF-κB-dependent luminescent signal in transgenic mice carrying the luciferase genes was used as the guide to monitor the biomaterials-affected organs, and transcriptomic analysis was further applied to evaluate the complex host responses in affected organs in this study. *In vivo* imaging showed that genipin-cross-linked gelatin conduit (GGC) implantation evoked the strong NF-κB activity at 6 h in the implanted region, and transcriptomic analysis showed that the expressions of interleukin-6 (IL-6), IL-24, and IL-1 family were up-regulated. A strong luminescent signal was observed in spleen on 14 d, suggesting that GGC implantation might elicit the biological events in spleen. Transcriptomic analysis of spleen showed that 13 Kyoto Encyclopedia of Genes and Genomes pathways belonging to cell cycles, immune responses, and metabolism were significantly altered by GGC implants. Connectivity Map analysis suggested that the gene signatures of GGC were similar to those of compounds that affect lipid or glucose

metabolism. GeneSetTest analysis further showed that host responses to GGC implants might be related to diseases states, especially the metabolic and cardiovascular diseases. In conclusion, our data provided a concept of molecular imaging-guided transcriptomic platform for the evaluation and the prediction of host–biomaterial interaction *in vivo*.

Keywords: Bioluminescence imaging; Transcriptomic analysis; Nuclear factor-κB; Genipin-cross-linked gelatin

1. Introduction

The establishment of a comprehensive platform for the prediction and the assessment of host–biomaterial interaction in vivo is an important issue. However, host–biomaterial interaction is a very complex process. Host responses to biomaterials control the biological performances of implanted medical devices and delivery vehicles. After the implantation of biomaterials, synthetic materials dynamically adsorb proteins and other biomolecules, which trigger an inflammatory cascade comprising blood coagulation, leukocyte recruitment and adhesion, foreign body reaction, and fibrous encapsulation [1] and [2]. Traditionally, standard cell-based toxicity assays are performed in vitro and the high-risk materials are removed at this early stage. Transcriptomic or proteomic analysis has also been used for understanding better the complexicity of cell–biomaterial interaction and to provide a comprehensive study of cell responses to biomaterials [3], [4] and [5]. Although these cell-based systems are excellent at defining single variable effects and responses, they are limited with respect to prediction of events that might occur in vivo [6].

Biocompatibility test for the biomaterials at both pre-clinical and clinical levels is based primarily on where and how long the materials will be used in the body. In addition to the inflammatory responses in the implanted regions, biomaterials may evoke various host responses in the body distinct from the implanted regions. However, it is difficult to know which internal organs distant from the implanted regions are altered by the biomaterial implants. Nuclear factor-κB (NF-κB) is an inducible transcript factor that consists of heterodimers of RelA (p65), c-Rel, RelB, p50, and p52. NF-κB plays a central coordinator of innate and adaptive immune responses. It also has a critical role in the development of cancer, regulation of cell apoptosis, and cell cycle regulation [7], [8] and [9]. When cells are exposed to stress, NF-κB translocates into the nucleus and binds to a unique decameric nucleotide sequence present in the promoter of various genes. NF-κB is activated by a large variety of signals, which typically include cytokines, mitogens, environmental particles, toxic metals, intracellular stresses, pathogen products, and ultraviolet light [10]. This property makes NF-κB a potent sensor to sense the affected cells in response to stress, and NF-κB-driven bioluminescence imaging may be used as a guide to monitor the affected organs.

In previous study, we have constructed the transgenic mice carrying the NF-κB-driven luciferase genes and have assessed the feasibility of noninvasive real-time NF-κB bioluminescence imaging on the evaluation of inflammation status in the implanted region [11]. In this study, we monitored the host responses after the implantation of genipin-cross-linked gelatin conduit (GGC) by bioluminescence imaging, and the host–biomaterials interaction was further interpreted by transcriptomic analysis. Our findings suggested that NF-κB-driven bioluminescence imaging-guided transcriptomic analysis may be used to analyze the host–biomaterial interaction in vivo.

2. Materials and methods

2.1. Materials

The GGC implant (1.96 mm in diameter, 1.5 mm in length) and lipopolysaccharide (LPS)-immersed GGC implant were prepared as described previously [11] and [12]. LPS was purchased from Sigma (St. Louis, MO) and dissolved in water at 5 mg/ml. d-Luciferin was purchased from Xenogen (Hopkinton, MA) and dissolved in phosphate-buffered saline (137 mm NaCl, 1.4 mm KH2PO4, 4.3 mm Na2HPO4, 2.7 mm KCl, pH 7.2) at 15 mg/ml. Rabbit polyclonal antibody against interleukin-1β (IL-1β) and goat polyclonal antibodies against IL-6 and IL-18 were purchased from Santa Cruz Biotechnology (Santa Cruz, CA).

2.2. Animal experiments

Mouse experiments were conducted under ethics approval from the China Medical University Animal Ethics Committee. Transgenic mice, carrying the luciferase gene driven by NF-κB-responsive elements, were constructed as described previously [11]. All transgenic mice were crossed with wild-type F1 mice to yield NF-κB-luc heterozygous mice with the FVB genetic background.

Transgenic mice were anesthetized with 0.12 g ketamine/kg body weight. For insertion of the implant, one incision (3 mm in length) on the back was made. LPS-immersed GGC or GGC was implanted subcutaneously into the incision and the skin was closed with silk sutures. A total of 12 transgenic mice was randomly divided into four groups of three mice: (1) sham, the incision was made and nothing was implanted; (2) LPS, the incision was made and LPS (5 μl of 5 mg/ml LPS) was dropped into the incision; (3) GGC, the incision was made and GGC was implanted; and (4) LPS-immersed GGC, the incision was made and LPS-immersed GGC was implanted. LPS and LPS-immersed GGC implants were used as positive controls to demonstrate strong responses in the transgenic mouse model system. Mice were imaged for the luciferase activity on the indicated periods and subsequently sacrificed for ex vivo imaging, immunohistochemical staining, and RNA extraction.

2.3. In vivo and ex vivo imaging of luciferase activity

For in vivo imaging, mice were anesthetized with isoflurane and injected intraperitoneally with 150 mg luciferin/kg body weight. Five minutes later, mice were placed facing down in the chamber and imaged for 5 min with the camera set at the highest sensitivity by IVIS Imaging System® 200 Series (Xenogen, Hopkinton, MA). Photons emitted from tissues were quantified using Living Image® software (Xenogen, Hopkinton, MA). Signal intensity was quantified as the sum of all detected photon counts per second within the region of interest after subtracting the background luminescence and presented as photons/sec/cm2/steradian (photons/s/cm2/sr).

For ex vivo imaging, mice were anesthetized and injected with luciferin intraperitoneally. Five minutes later, mice were sacrificed and tissues were rapidly removed. Tissues were placed in the IVIS system and imaged with the same setting used for in vivo studies. Signal intensity was quantified as the sum of all detected photon counts from tissues and presented

as photons/s.

2.4. Total RNA extraction

Total RNAs were extracted from spleens or tissues around implanted regions using RNeasy Mini kit (Qiagen, Valencia, CA). Total RNA was quantified using the Beckman DU800 spectrophotometer (Beckman Coulter, Fullerton, CA). Samples with A260/A280 ratios greater than 1.8 were further evaluated using Agilent 2100 bioanalyzer (Agilent Technologies, Santa Clara, CA). The RNA samples with a RNA integrity number greater than 8.0 were accepted for microarray analysis.

2.5. Microarray analysis

Microarray analysis was performed as described previously [13] and [14]. Briefly, fluorescence-labeled RNA targets were prepared from 5 μg of total RNA using MessageAmp™ aRNA kit (Ambion, Austin, TX) and Cy5 dye (Amersham Pharmacia, Piscataway, NJ). Fluorescent targets were hybridized to the Mouse Whole Genome OneArray™ (Phalanx Biotech Group, Hsinchu, Taiwan) and scanned by an Axon 4000 scanner (Molecular Devices, Sunnyvale, CA). Number of replicates was three. The Cy5 fluorescent intensity of each spot was analyzed by genepix 4.1 software (Molecular Devices, Sunnyvale, CA). The signal intensity of each spot was corrected by subtracting background signals in the surrounding. We filtered out spots that signal-to-noise ratio was less than 1 or control probes. Spots that passed these criteria were normalized by the limma package of the R program [15]. We analyzed the expression levels of cytokine genes in the implanted regions at 6 h and on 14 d post-implantation. Additionally, genes with fold changes >2.5 in spleen were analyzed by Kyoto Encyclopedia of Genes and Genomes (KEGG) PATHWAY (http://www.genome.ad.jp/kegg/), which is a knowledge base linking a set of genes in the genome with a network of interacting molecules in the cells [16]. We used the WebGestalt tool to test significant KEGG pathways. Furthermore, we constructed the interaction network of these genes using BiblioSphere Pathway Edition software (http://www.genomatix.de/index.html), which is a knowledge base integrating literature mining and annotation analysis with promoter sequence analysis [17]. Finally, we used the cytoscape software to find out and to visualize the interaction network of up-regulated genes, which are relative to NF-κB [18].

2.6. Connectivity Map analysis of GGC-altered genes and drugs-altered genes

To connect the expression signatures of GGC-altered genes with those of drugs-regulated genes, we analyzed gene expression profiles by the Connectivity Map [19]. We first converted the symbols of genes with fold changes >2.5 in spleen into Affymetrix ID according to U133A probe set. Then, we uploaded and analyzed these gene lists on the Connectivity Map (http://www.broad.mit.edu/cmap/). Using Connectivity Map, an imported query was

compared with predefined signatures of therapeutic compounds and ranked according to a connectivity score, representing relative similarity to the imported gene lists.

2.7. Connection analysis of GGC-altered genes and disease-related genes

To connect the gene expression profile of GGC implantation with that of disease, we built the diseases-genes database from the genetic association database according to Medical Subject Headings (MeSH) terms (http://www.nlm.nih.gov/mesh/meshhome.html) [20]. We used the "geneSetTest" function implemented in the limma package of the R program to detect groups of genes in MeSH disease terms. This function computes a p-value to test the hypothesis that the selected genes tend to be up-regulated or down-regulated. Then, we defined the score for each gene set as the negative logarithm of its p-value computed by "geneSetTest" function.

2.8. Immunohistochemical staining

Sections of 5 μm were deparaffinized in xylene and rehydrated in graded alcohol. Endogenous peroxidase was quenched with 3% hydrogen peroxide in methanol for 15 min and the nonspecific binding was blocked with 1% bovine serum albumin at room temperature for 1 h. Sections were incubated with antibodies against cytokines at 1:50 dilution overnight at 4 °C and then incubated with biotinylated secondary antibody (Zymed Laboratories South San Francisco, CA) at room temperature for 20 min. Finally, slides were incubated with avidin–biotin complex reagent and stained with 3,3′-diaminobenzidine according to manufacturer's protocol (Histostain®-Plus kit, Zymed Laboratories).

2.9. Statistical analysis

Data were presented as mean ± standard error. Student's t test was used for comparisons between two experiments. A value of $p < 0.05$ was considered statistically significant.

3. Results

3.1. Assessment of the NF-κB-driven bioluminescent signal in GGC-implanted mice by in vivo and ex vivo imaging

The GGC or LPS-immersed GGC implant was implanted subcutaneously in the dorsal region and the NF-κB-driven bioluminescent signals were monitored by luminescent imaging on the indicated periods (Fig. 1). In consistent with previous study [11], luminescent signal in the implanted region was initially increased and gradually decreased in all groups. NF-κB activity reached a maximal activation at 6 h. At 6 h post-implantation, a strong and specific in vivo bioluminescence around the incision was observed in LPS (1.84 × 106 photons/s/cm2/sr) and LPS-immersed GGC groups (1.56 × 106 photons/s/cm2/sr), while a moderate signal was evoked in the GGC group (0.63 × 106 photons/s/cm2/sr). On 14 d, the luminescent signal was decreased in GGC groups. These data indicated that the implantation of LPS-immersed GGC, as expected, induced a strong NF-κB activity, while GGC implant, which has been demonstrated to evoke a mild tissue response [12], induced a weak signal compared with the

LPS-immersed GGC implant.

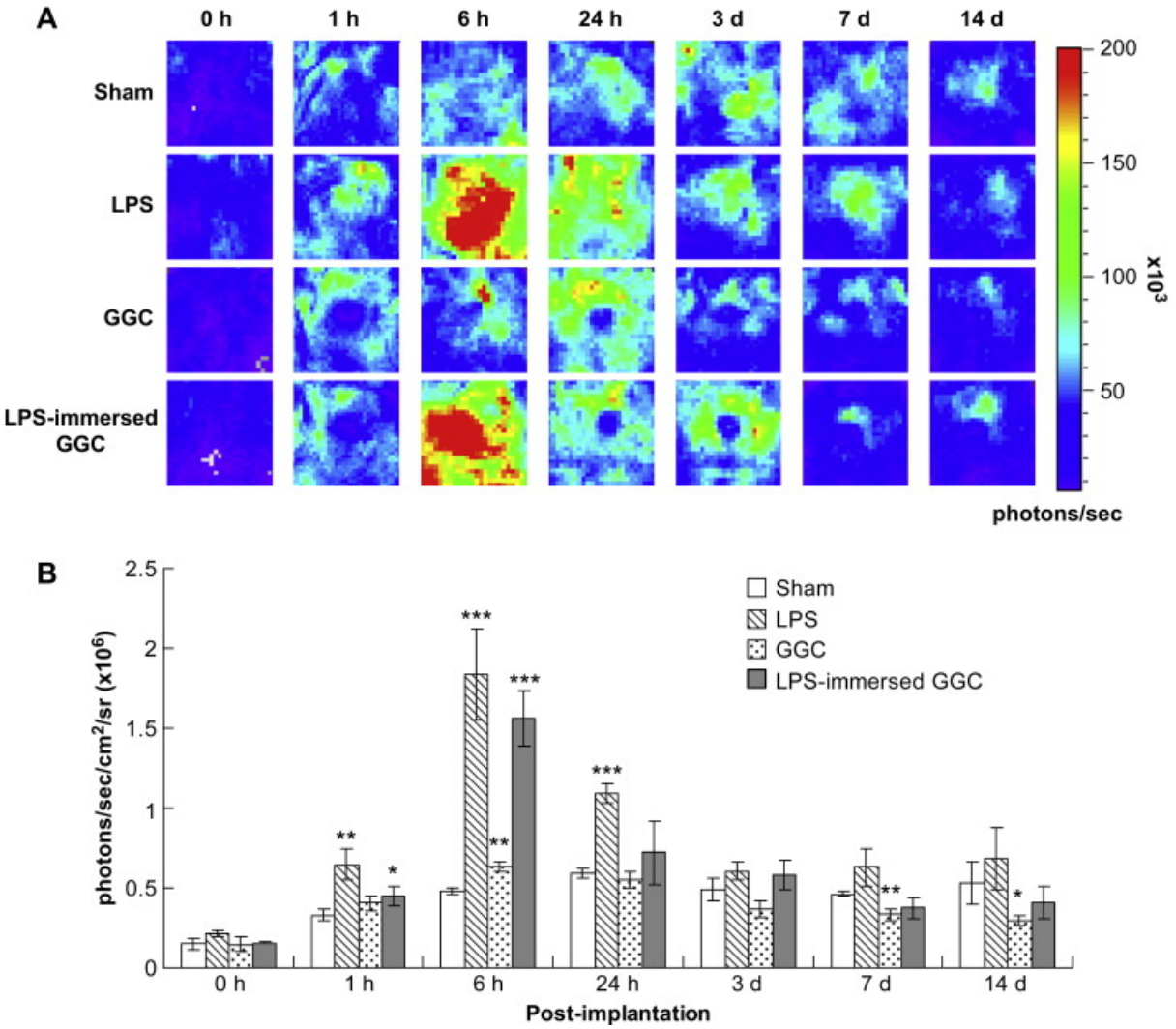

Fig. 1. NF-κB-dependent bioluminescence in living mice implanted with GGC and LPS-immersed GGC. Transgenic mice were randomly divided into four groups of three mice. The in vivo imaging was obtained at indicated periods. (A) Diagrams show the bioluminescent signal within a radius of 2.5 mm of implanted region. The color overlay on the image represents the photons/s emitted from the animal, as indicated by the color scales. (B) Quantification of photon emission within the implanted region. Values are mean ± standard error of three mice. *$p < 0.05$, **$p < 0.01$, ***$p < 0.001$, compared with sham.

Because biomaterials might evoke various host responses in the body distinct from the implanted regions, we applied the ex vivo bioluminescent imaging to monitor the affected organs on 14 d post-implantation (Fig. 2). In consistent with in vivo imaging data, the luminescent signal in the implanted region was significantly decreased in GGC group compared with sham. LPS significantly evoked the luminescent signals in the liver, spleen, kidney, and small intestine, while GGC significantly elicited the luminescence in the spleen. These data suggested that, in addition to implanted area, GGC implantation affected NF-κB

activities in internal organs, especially the spleen. Therefore, we further analyzed the gene expression profiles of implanted regions and spleen to evaluate the host–GGC interaction by transcriptomic analysis.

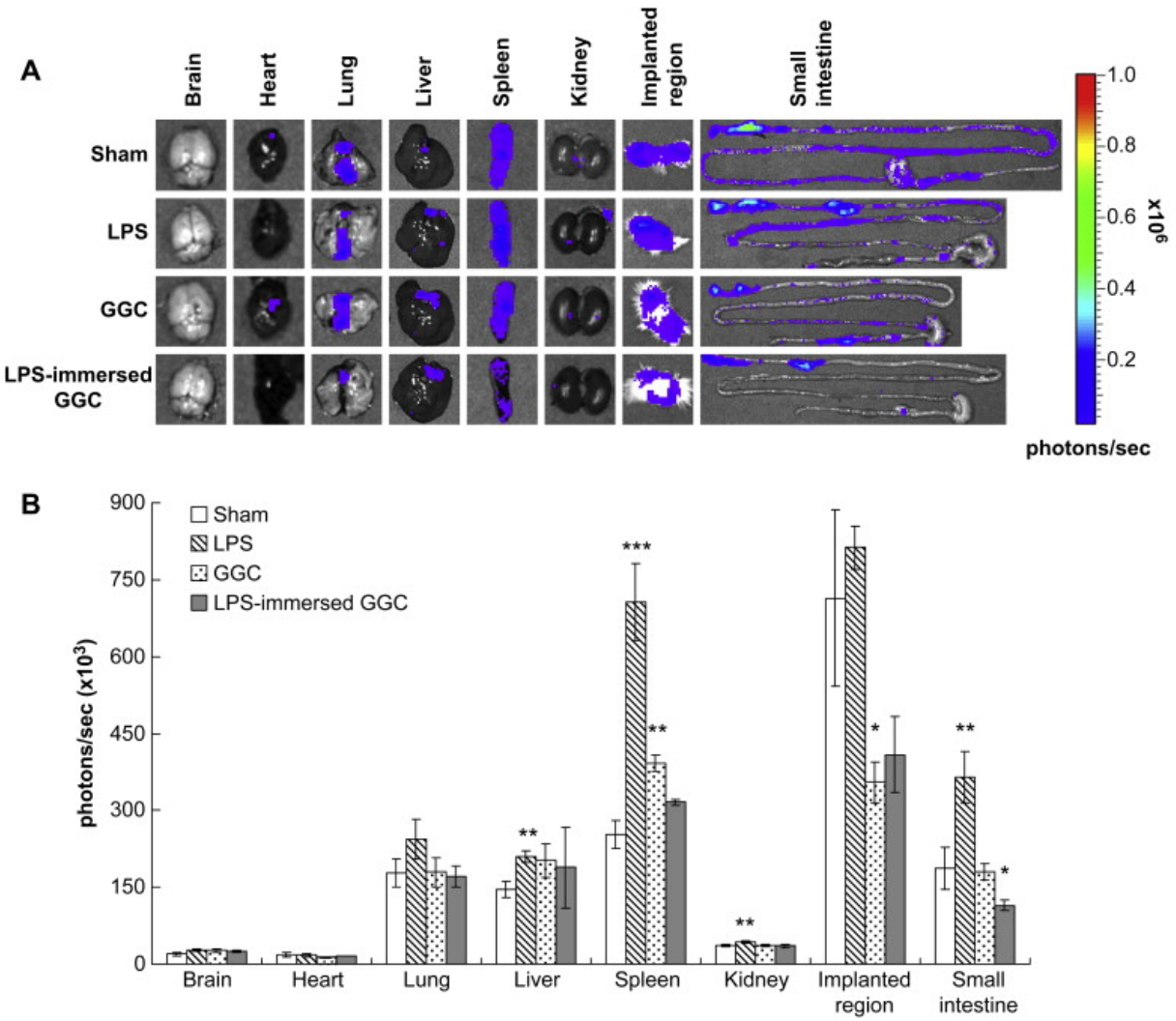

Fig. 2. NF-κB-dependent bioluminescence in individual organs. Transgenic mice were randomly divided into four groups of three mice. On 14 d after implantation, mice were injected intraperitoneally with d-luciferin. Five minutes later, mice were sacrificed, and the organs were excised rapidly and subjected to image. (A) Ex vivo imaging. The color overlay on the image represents the photons/s emitted from the organs, as indicated by the color scales. (B) Quantification of photon emission in the organ. Values are mean ± standard error of three mice. *p < 0.05, **p < 0.01, ***p < 0.001, compared with sham.

3.2. Expression levels of cytokine genes in GGC-implanted regions

We first analyzed the inflammatory responses of implanted regions after a short-term (6 h) and a long-term (14 d) implantation by transcriptomic analysis. The expression levels of cytokine genes are shown in Table 1. At 6 h post-implantation, the expressions of IL-6, IL-24, and IL-1 family, such as IL-1β, IL-18 and IL-33, were up-regulated at least 2-fold in the

GGC-implanted regions. Immunohistochemical staining using anti-IL-1β, IL-6, and IL-18 antibodies further showed that, in comparison with sham, there were many brown immuno-reactive cells in the GGC-implanted regions (Fig. 3). On 14 d post-implantation, the expressions of all cytokine genes were slightly affected by GGC in the implanted region and spleen (data not shown). The increased NF-κB-dependent luminescent signal was correlated with the increased number of affected genes. These findings suggested that bioluminescence imaging-guided transcriptomic analysis might reflect the host responses to GGC implants in the implanted region.

Table 1.

Expression levels of cytokine genes in the implanted regions at 6 h and on 14 d post-implantation by transcriptomic analysis.

Gene	Fold changes	
	6 h	14 d
Interleukin 1 alpha	1.12 ± 0.04	−1.04 ± 0.05
Interleukin 1 beta	8.93 ± 2.53	1.05 ± 0.07
Interleukin 1 family, member 5 (delta)	2.78 ± 0.59	−1.05 ± 0.06
Interleukin 1 family, member 6	10.46 ± 1.48	−1.04 ± 0.03
Interleukin 1 family, member 8	1.50 ± 0.40	−1.04 ± 0.07
Interleukin 1 family, member 9	6.19 ± 1.35	−1.04 ± 0.06
Interleukin 1 family, member 10	1.33 ± 0.25	1.00 ± 0.02
Interleukin 2	−1.05 ± 0.03	1.00 ± 0.03
Interleukin 3	1.01 ± 0.03	−1.01 ± 0.03
Interleukin 4	1.03 ± 0.05	1.02 ± 0.04
Interleukin 5	−1.09 ± 0.04	1.06 ± 0.12
Interleukin 6	6.68 ± 2.10	1.02 ± 0.03
Interleukin 7	1.09 ± 0.14	1.04 ± 0.05
Interleukin 9	−1.07 ± 0.04	−1.03 ± 0.04
Interleukin 10	1.13 ± 0.08	1.03 ± 0.03
Interleukin 12a	−1.33 ± 0.29	1.09 ± 0.06
Interleukin 12b	1.00 ± 0.07	1.01 ± 0.03
Interleukin 13	1.11 ± 0.07	−1.10 ± 0.05
Interleukin 15	1.14 ± 0.11	1.03 ± 0.03
Interleukin 16	1.32 ± 0.06	1.02 ± 0.22
Interleukin 17A	1.08 ± 0.07	1.02 ± 0.05
Interleukin 17B	−1.28 ± 0.13	1.06 ± 0.15

Gene	Fold changes	
	6 h	14 d
Interleukin 17C	−1.07 ± 0.28	1.19 ± 0.33
Interleukin 17D	−1.07 ± 0.05	1.01 ± 0.06
Interleukin 17F	1.02 ± 0.12	1.65 ± 0.36
Interleukin 18	4.20 ± 0.93	−1.21 ± 0.12
Interleukin 20	1.04 ± 0.16	1.01 ± 0.16
Interleukin 21	1.04 ± 0.07	1.00 ± 0.05
Interleukin 22	1.06 ± 0.03	−1.03 ± 0.01
Interleukin 23, alpha subunit p19	−1.06 ± 0.06	−1.04 ± 0.05
Interleukin 24	2.02 ± 0.54	−1.02 ± 0.04
Interleukin 25	−1.05 ± 0.06	1.03 ± 0.05
Interleukin 27	−1.07 ± 0.10	1.07 ± 0.12
Interleukin 28	−1.02 ± 0.04	1.05 ± 0.04
Interleukin 31	1.01 ± 0.03	1.01 ± 0.04
Interleukin 33	4.28 ± 0.86	1.21 ± 0.16

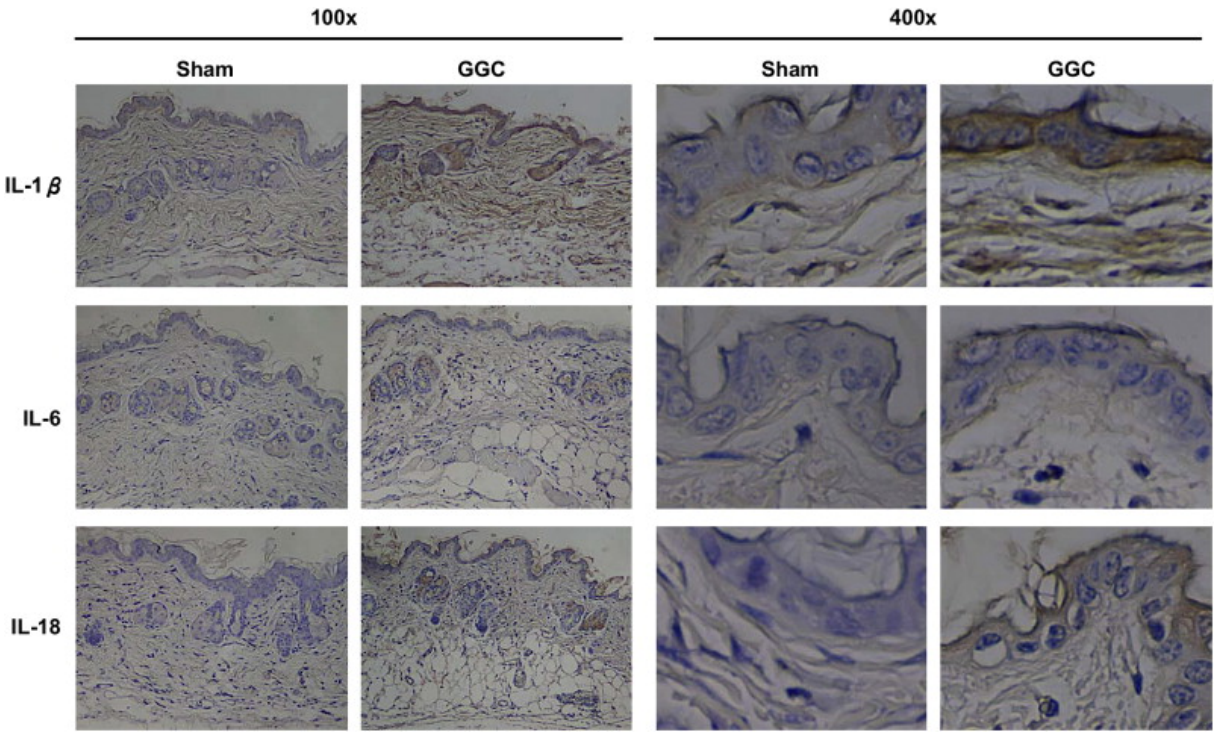

Fig. 3. Immunohistochemical examinations of tissues implanted without or with GGC. Transgenic mice were implanted without (sham) or with GGC in the dorsal region. On 14 d post-implantation, tissues around the implants were excised, and the sections were stained by

immunohistochemistry using antibodies against IL-1β, IL-6, or IL-18 (100× and 400× magnification). Similar results were obtained from three independent experiments.

3.3. Transcriptomic analysis of host–GGC interaction in spleen

On 14 d post-implantation, GGC implants significantly evoked the NF-κB-dependent bioluminescence in spleen. Therefore, we elucidated the host responses to GGC in spleen by transcriptomic analysis. In a total of 29,922 genes, 8583 genes, which passed the criteria described in Section 2, were selected, and genes with fold changes >2.5 were further classified by KEGG PATHWAY. KEGG PATHWAY analysis showed that 19 pathways, in which more than 15 genes were affected, were altered (Table 2). Among 19 pathways, 13 pathways involved in cell cycles, immune responses, or metabolism were significantly altered in spleen. Moreover, 5 pathways, including regulation of actin cytoskeleton, ribosome, focal adhesion, leukocyte transendothelial migration and insulin signaling pathway, were significantly affected in both spleen and implanted regions. We further constructed the interaction network of GGC-altered genes by BiblioSphere Pathway Edition software and visualized the connection by cytoscape software (Fig. 4). Most genes were connected with NF-κB, suggesting that NF-κB played a central role in the network. These findings also suggested the coincidence of NF-κB-driven imaging and transcriptomic data on the analysis of gene expression profiles.

Table 2.
Classification of GGC-altered genes by KEGG PATHWAY.

KEGG PATHWAY[3]	Gene number	
	Spleen	Implanted regions
MAPK signaling pathway	38	13
Regulation of actin cytoskeleton	37***	17**
Ribosome	37***	14***
Focal adhesion	34**	19**
Oxidative phosphorylation	32***	9
Cell cycle	30***	5
Purine metabolism	26**	10
Leukocyte transendothelial migration	25***	11*
Insulin signaling pathway	23*	14**
Tight junction	23**	8
T cell receptor signaling pathway	22***	3

KEGG PATHWAY[3]	Gene number	
	Spleen	Implanted regions
Wnt signaling pathway	21	13*
Axon guidance	20	5
Pyrimidine metabolism	18**	6
Jak-STAT signaling pathway	17	6
Gap junction	17*	3
Cell Communication	16	19***
Chronic myeloid leukemia	16**	1
Natural killer cell mediated cytotoxicity	15	3

*p < 0.05, **p < 0.01, and ***p < 0.001 were calculated by hypergeometric test on Gene Ontology Tree Machine web site (http://bioinfo.vanderbilt.edu/gotm/).

a Genes with fold changes >2.5 were analyzed by KEGG PATHWAY.

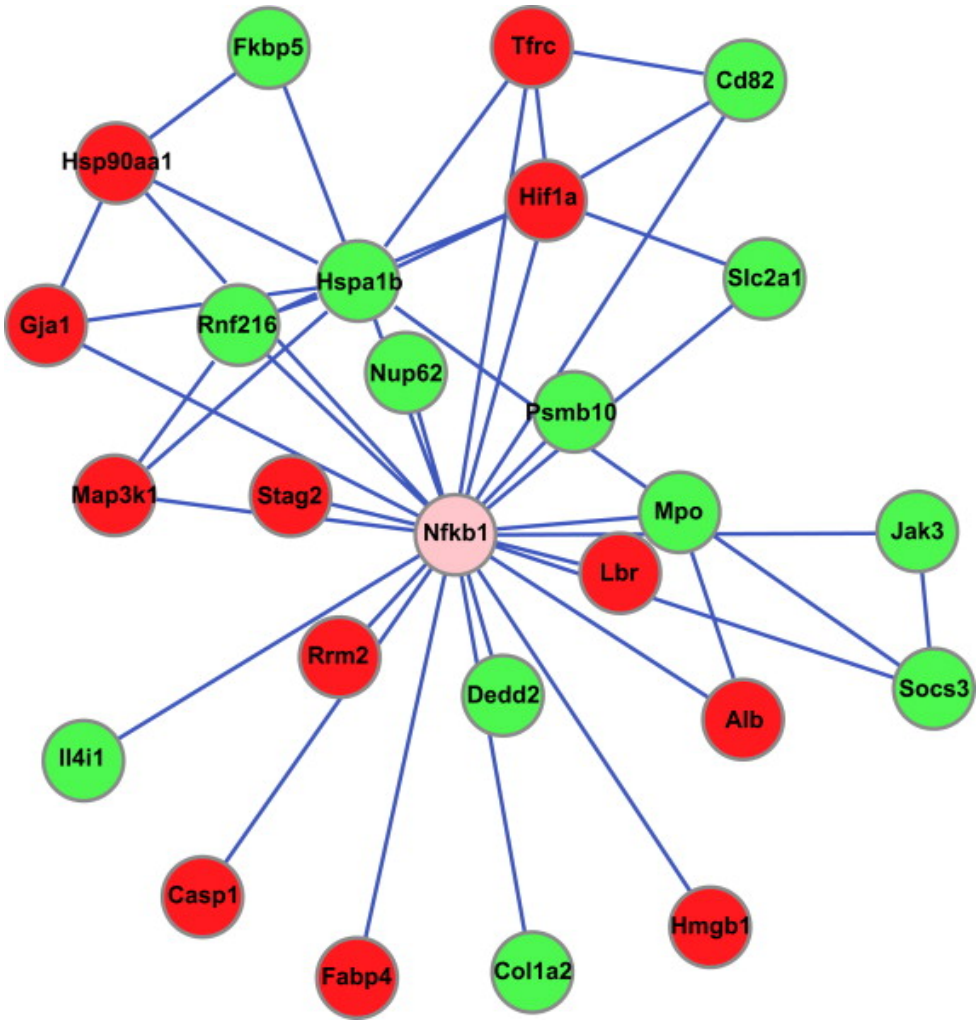

Fig. 4. Network analysis of GGC-altered genes in spleen on 14 d post-implantation. Genes with fold changes >2.5 were selected and analyzed by BiblioSphere Pathway Edition software. The connection between NF-κB and GGC-altered genes was visualized by cytoscape software. Up-regulated genes are colored red and down-regulated genes are colored green.

3.4. Gene expression connection between host–GGC interaction and drugs

To further evaluate whether the host responses of GGC were similar to those of drugs, we connected the gene expression signatures by Connectivity Map. Genes with fold changes >2.5 were selected and analyzed to obtain the connectivity score. Connectivity Map links genes associated with a phenotype with potential therapeutic agents. Using Connectivity Map, an imported query is compared with predefined signatures of therapeutic compounds and ranks according to a connectivity score. A connectivity score from +1 to −1 is assigned based on the degree of similarity or dissimilarity between the two experiments. A drug with a high connectivity score has a gene signature very similar to the query signature. The top ten drugs with high connectivity scores are shown in Table 3. Over half of drugs or compounds have been shown to be involved in lipid or glucose metabolism. These drugs or compounds include estradiol, chlorpropamide, arachidonyltrifluoromethane, LY-294002, valproic acid, and alpha-estradiol. Therefore, these findings suggested that the host responses induced by GGC were related to drugs, which are involved in lipid or glucose metabolism.

Table 3.
Connectivity Map analysis of host–GGC interaction and drugs.

cmap name	Connectivity score	Up scorea	Down scoreb
Estradiol	1	0.18	−0.165
Chlorpropamide	0.986	0.231	−0.109
Arachidonyltrifluoromethane	0.971	0.185	−0.15
17-Allylamino-geldanamycin	0.945	0.159	−0.167
LY-294002	0.936	0.171	−0.152
12,13-EODE	0.925	0.214	−0.105
Monorden	0.913	0.205	−0.11
Geldanamycin	0.864	0.152	−0.146
Valproic acid	0.852	0.22	−0.074
Alpha-estradiol	0.846	0.197	−0.095

a A value between +1 and −1 represented the absolute enrichment of up-regulated query genes in a given instance.

b A value between +1 and −1 represented the absolute enrichment of down-regulated query genes in a given instance.

3.5. Gene expression connection between host–GGC interaction and disease states

We next tested groups of altered genes in MeSH disease terms by the "geneSetTest" to interpret whether the host responses induced by GGC were related to diseases states. Among 735 tested MeSH disease terms, 12 terms with score >1.5 or <−1.5 are shown in Table 4. We further classified 12 MeSH disease terms in to 4 kinds of diseases, including metabolic and cardiovascular diseases, nervous and musculoskeletal diseases, neoplasms, and others. More than half of the MeSH disease terms were relative to the metabolic and cardiovascular diseases. These findings suggested that the host responses to GGC implantation might be related to diseases states, especially the metabolic and cardiovascular diseases.

Table 4.

Gene expression connection between host–GGC interaction and disease states.

MeSH disease term	Scorea	p-value	Classification
Hyperglycemia	−2.3923	0.0041	Metabolic and cardiovascular diseases
Muscular dystrophies	−2.0317	0.0093	Nervous and musculoskeletal diseases
Sarcoidosis	−1.9286	0.0118	Metabolic and cardiovascular diseases
Huntington disease	1.9135	0.0122	Nervous and musculoskeletal diseases
Hyperinsulinism	−1.8049	0.0157	Metabolic and cardiovascular diseases
Keratosis	−1.7175	0.0192	Others
Congestive heart failure	−1.7171	0.0192	Metabolic and cardiovascular diseases
Adenoma	1.7086	0.0196	Neoplasms
Cell transformation	−1.6712	0.0213	Neoplasms
Raynaud's disease	−1.5932	0.0255	Metabolic and cardiovascular diseases
Muscular diseases	1.5092	0.0310	Nervous and musculoskeletal diseases
Medulloblastoma	1.5089	0.0310	Neoplasms

Full-size table

a The value was calculated as the negative logarithm of p-value by "getSetTest" function.

4. Discussion

In previous study, we have demonstrated the feasibility of NF-κB-driven bioluminescence imaging for the evaluation of host–biomaterials interaction in implanted region [11]. In this study, we applied the bioluminescence imaging to monitor the implanted region and internal organs that were affected by GGC implantation. The complex host responses to biomaterials were further interpreted and predicted by transcriptomic analysis. Transcriptomic analysis by DNA microarray tools has evolved rapidly since its introduction in 1995 [21]. Microarray is a

popular research and screening tool for differentially expressed genes. Microarray-based gene expression patterns have been used to predict the candidate biomarkers, to predict the therapeutic efficacies of drugs, to predict the clinical outcomes, to recognize the toxic potential of drug candidate, and to find connections among small molecules, genes, and diseases [19], [22] and [23]. They have also been used to analyze the cell responses to biomaterials in vitro and the host responses to biomaterials in the implant-associated tissues [3], [4], [5] and [24].

To elucidate the inflammatory responses to GGC implants, the expression levels of cytokine genes in the implanted region were evaluated by transcriptomic tools. The expressions of IL-1β, IL-18, IL-33, IL-6, and IL-24 were up-regulated at least 2-fold at 6 h post-implantation. IL-1β, IL-6, and IL-24 genes are usually produced at the site of inflammation in response to infection. IL-24 acts on non-haematopoietic tissues and performs an important role in wound healing [25]. The up-regulation of IL-24 gene suggested that the wound healing process was evoked in the implanted region at 6 h. IL-6 is involved in the induction of acute phase proteins and the development of fever. IL-6, in combination with its soluble receptor, dictates the transition from acute to chronic inflammation [26]. The up-regulation of IL-6 gene suggested that GGC implantation might evoke the chronic inflammatory responses. IL-1β, IL-18, and IL-33 belong to the IL-1 family of cytokines. IL-1β is a proinflammatory cytokine. It plays a critical role in the regulation of the immune response and inflammation, and induces the production of other proinflammatory cytokines, such as IL-6 [27]. IL-18 acts on T helper type 1 cells and in combination with IL-12 strongly induces the production of interferon-γ. It also induces natural killer cell activity in spleen [27]. IL-33 functions as both a proinflammatory cytokine and an intracellular nuclear factor involved in transcriptional regulation [28]. The up-regulations of IL-1 family and IL-6 at 6 h post-implantation suggested that GGC elicited acute inflammation in the implanted region.

In addition to the host responses in the implanted region, we would like to know whether the internal organs distant from the implanted regions were altered by the GGC implants. NF-κB-driven bioluminescence imaging was therefore used as a guide to monitor the affected organs. A strong luminescent signal driven by NF-κB activity was observed in spleen, suggesting that GGC implantation altered the biological events in the spleen. Transcriptomic analysis showed that GGC implants affected cell cycle, immune response, and metabolism pathways, which have been known to be regulated by NF-κB activity in spleen. Network analysis of GGC-altered genes in spleen further showed that NF-κB played a central role in the network. The correlation between NF-κB-dependent bioluminescence and NF-κB-regulated biological events emphasized the feasibility of NF-κB bioluminescence-guided transcriptomic analysis on the evaluation and prediction of host–biomaterials interaction in vivo.

Connectivity Map is a method that compares lists of differential expressed genes to a library of experiments assessing the effects of small molecules and genetic events on gene expression

[19] and [29]. Connectivity Map finds connections among molecules sharing similar mechanisms of action. Connectivity Map has been applied to identify drugs, pathways, and mechanisms. For examples, Connectivity Map has been used to identify pathways associated with chemotherapy resistance [30]. It has also been applied to identify drugs that induce p75 activity and eradicate leukemia stem cells [31]. In this study, we applied Connectivity Map to link GGC-altered genes associated with drugs or compounds. By connecting the gene expression signature of GGC with that of drug, we found that the gene expression profile induced by GGC was similar to those induced by lipid or glucose metabolism-associated compounds, such as estradiol, chlorpropamide, arachidonyltrifluoromethane, LY-294002, valproic acid, and alpha-estradiol. Estradiol, a sex hormone, regulates the catalytic activity of lipoprotein lipase, promotes leptin expression in human adipose tissue, and increases pre-adipocyte proliferation in vitro [32]. It also induces insulin resistance in vitro and in vivo [33] and [34]. Chlorpropamide is a sulfonylurea hypoglycemic agent that has been used in the treatment of non-insulin-dependent diabetes mellitus [35]. Arachidonyltrifluoromethane, a trifluoromethyl ketone analogue of arachidonic acid, is a tight- and slow-binding inhibitor of phospholipase A2. Is also stimulates glucose uptake and inhibits lipogenic gene expression in adipocytes [36] and [37]. LY-294002 is a phosphoinositide-3-kinase inhibitor that inhibits the insulin-stimulated glucose uptake [38]. Valproic acid is a fatty acid that has been used in the treatment of epilepsy. It inhibits the expression of adiponectin, which plays an important role in controlling insulin sensitivity and glucose homeostasis [39]. It also inhibits leptin secretion and blocks adipogenesis in adipocytes [40]. Connectivity Map analysis suggested that gene signatures of GGC were similar to the gene signatures of compounds that are involved in lipid or glucose metabolism. GeneSetTest analysis also suggested that host responses to GGC implants might be related to diseases states, especially the metabolic and cardiovascular diseases. Interestingly, geniposide, the precursor of genipin, has been proven to inhibit phospholipase A2 activity in vitro and play a role in adipogenesis [41]. Genipin has been shown to exhibit antithrombotic effect by prolonging the time required for thrombotic occlusion in the mouse femoral artery [41]. Moreover, genipin has been shown to inhibit uncoupling protein 2-mediated protein leak and to reverse obesity- and high glucose-induced beta cell dysfunction in isolated pancreatic islets [42]. The predicted host responses to GGC implants by NF-κB bioluminescence imaging-guided transcriptomic analysis are similar to the previous data of genipin. These findings suggested that NF-κB bioluminescence imaging-guided transcriptomic analysis could be used to predict and interpret the long-term interaction between host and biomaterials in vivo.

5. Conclusion

NF-κB is activated by a variety of stimuli. NF-κB bioluminescent imaging was therefore used as a guide to monitor the affected internal organs after GGC implantation. Transcriptomic analysis was further applied to evaluate and predict the complex host responses in GGC implant-affected organs. Our data provides a concept of molecular imaging-guided

transcriptomic platform for the evaluation and the prediction of host–biomaterial interaction in vivo.

Acknowledgements

We thank Miss Hsin-Yi Lo, Mr. Chia-Cheng Li, and Mr. Wei-Shuen Shen for their technical assistances. This work was supported by grants from National Research Program for Genomic Medicine, National Science and Technology Program for Agricultural Biotechnology, National Science Council, Committee on Chinese Medicine and Pharmacy, Department of Health (CCMP 96-RD-201 and CCMP 97-RD-201), and China Medical University (CMU97-064 and CMU97-CMC-004), Taiwan.

References

[1] J.M. Anderson, Biological responses to materials, Annu Rev Mater Res 31 (2001), pp. 81–110.
[2] D.F. Williams, On the mechanisms of biocompatibility, Biomaterials 29 (2008), pp. 2941–2953.
[3] C.M. Klapperich and C.R. Bertozzi, Global gene expression of cells attached to a tissue engineering scaffold, Biomaterials 25 (2004), pp. 5631–5641.
[4] W.M. Gallagher, I. Lynch, L.T. Allen, I. Miller, S.C. Penney and D.P. O'Connor et al., Molecular basis of cell–biomaterial interaction: insights gained from transcriptomic and proteomic studies, Biomaterials 27 (2006), pp. 5871–5882.
[5] X. Lü, X. Bao, Y. Huang, Y. Qu, H. Lu and Z. Lu, Mechanisms of cytotoxicity of nickel ions based on gene expression profiles, Biomaterials 30 (2009), pp. 141–148.
[6] J.A. Hunt, P.J. McLaughlin and B.F. Flanagan, Techniques to investigate cellular and molecular interactions in the host response to implanted biomaterials, Biomaterials 18 (1997), pp. 1449–1459.
[7] A.S. Baldwin Jr., The NF-κB and IκB proteins: new discoveries and insights, Annu Rev Immunol 14 (1996), pp. 649–683.
[8] F. Chen, V. Castranova and X. Shi, New insights into the role of nuclear factor-κB in cell growth regulation, Am J Pathol 159 (2001), pp. 387–397.
[9] M.S. Hayden and S. Ghosh, Shared principles in NF-κB signaling, Cell 132 (2008), pp. 344–362.
[10] M. Karin and Y. Ben-Neriah, Phosphorylation meets ubiquitination: the control of NF-κB activity, Annu Rev Immunol 18 (2000), pp. 621–663.
[11] T.Y. Ho, Y.S. Chen and C.Y. Hsiang, Noninvasive nuclear factor-κB bioluminescence imaging for the assessment of host–biomaterial interaction in transgenic mice, Biomaterials 28 (2007), pp. 4370–4377.
[12] Y.S. Chen, J.Y. Chang, C.Y. Cheng, F.J. Tsai, C.H. Yao and B.S. Liu, An in vivo evaluation of a biodegradable genipin-cross-linked gelatin peripheral nerve guide conduit

material, Biomaterials 26 (2005), pp. 3911–3918.
[13] W.Y. Cheng, C.Y. Hsiang, D.T. Bau, J.C. Chen, W.S. Shen and C.C. Li et al., Microarray analysis of vanillin-regulated gene expression profile in human hepatocarcinoma cells, Pharm Res 56 (2007), pp. 474–482. Article |
[14] W.Y. Cheng, S.L. Wu, C.Y. Hsiang, C.C. Li, T.Y. Lai and H.Y. Lo et al., Relationship between San-Huang-Xie-Xin-Tang and its herbal components on the gene expression profiles in HepG2 cells, Am J Chin Med 36 (2008), pp. 783–797.
[15] G.K. Smyth, Limma: linear models for microarray data New York. In: R. Gentleman, V. Carey, S. Dudoit, R. Irizarry and W. Huber, Editors, Bioinformatics and computational biology solutions using R and bioconductor (2005), pp. 397–420.
[16] M. Kanehisa, Linking databases and organisms: genomenet resources in Japan, Trends Biochem Sci 22 (1997), pp. 442–444.
[17] M. Seifert, M. Scherf, A. Epple and T. Werner, Multievidence microarray mining, Trends Genet 21 (2005), pp. 553–558.
[18] P. Shannon, A. Markiel, O. Ozier, N.S. Baliga, J.T. Wang and D. Ramage et al., Cytoscape: a software environment for integrated models of biomolecular interaction networks, Genome Res 13 (2003), pp. 2498–2504.
[19] J. Lamb, E.D. Crawford, D. Peck, J.W. Modell, I.C. Blat and M.J. Wrobel et al., The Connectivity Map: using gene-expression signatures to connect small molecules, genes, and disease, Science 313 (2006), pp. 1929–1935.
[20] K.G. Becker, K.C. Barnes, T.J. Bright and S.A. Wang, The genetic association database, Nat Genet 36 (2004), pp. 431–432.
[21] M. Schena, D. Shalon, R.W. Davis and P.O. Brown, Quantitative monitoring of gene expression patterns with a complementary DNA microarray, Science 270 (1995), pp. 467–470.
[22] U. Scherf, D.T. Ross, M. Waltham, L.H. Smith, J.K. Lee and L. Tanabe et al., A gene expression database for the molecular pharmacology of cancer, Nat Genet 24 (2000), pp. 236–244.
[23] E.C. Gunther, D.J. Stone, R.W. Gerwien, P. Bento and M.P. Heyes, Prediction of clinical drug efficacy by classification of drug-induced genomic expression profiles in vitro, Proc Natl Acad Sci U S A 100 (2003), pp. 9608–9613.
[24] N. Kojima, S. Ozawa, Y. Miyata, H. Hasegawa, Y. Tanaka and T. Ogawa, High-throughput gene expression analysis in bone healing around titanium implants by DNA microarray, Clin Oral Implants Res 19 (2008), pp. 173–181.
[25] M. Wang and P. Liang, Interleukin-24 and its receptors, Immunology 114 (2005), pp. 166–170.
[26] C. Gabay, Interleukin-6 and chronic inflammation, Arthritis Res Ther 8 (2006), p. S3.
[27] N. Delaleu and M. Bickel, Interleukin-1β and interleukin-18: regulation and activity in local inflammation, Periodontology 2004 (35) (2000), pp. 42–52.

[28] R. Kakkar and R.T. Lee, The IL-33/ST2 pathway: therapeutic target and novel biomarker, Nat Rev Drug Discov 7 (2008), pp. 827–840.
[29] J. Lamb, The Connectivity Map: a new tool for biomedical research, Natl Rev 7 (2007), pp. 54–60.
[30] R.F. Riedel, A. Porrello, E. Pontzer, E.J. Chenette, D.S. Hsu and B. Balakumaran et al., A genomic approach to identify molecular pathways associated with chemotherapy resistance, Mol Cancer Ther 7 (2008), pp. 3141–3149.
[31] J.M. Rosenbluth, D.J. Mays, M.F. Pino, L.J. Tang and J.A. Pietenpol, A gene signature-based approach identifies mTOR as a regulator of p73Δ, Mol Cell Biol 28 (2008), pp. 5951–5964.
[32] M.N. Dieudonné, M.C. Leneveu, Y. Giudicelli and R. Pecquery, Evidence for functional estrogen receptors alpha and beta in human adipose cells: regional specificities and regulation by estrogens, Am J Physiol Cell Physiol 286 (2004), pp. C655–C661.
[33] M. Collison, I.W. Campbell, I.P. Salt, A.F. Dominiczak, J.M. Connell and H. Lyall et al., Sex hormones induce insulin resistance in 3T3-L1 adipocytes by reducing cellular content of IRS proteins, Diabetologia 43 (2000), pp. 1374–1380.
[34] Y. Wen, H. Wang, R. MacLaren, H. Lu, X.F. Hu and K. Cianflone, Sex steroid hormones induce acylation stimulating protein resistance in 3T3-L1 adipocytes, J Cell Biochem 105 (2008), pp. 404–413.
[35] A.K. Diehl, N.J. Sugarek and R.L. Bauer, Medication compliance in non-insulin-dependent diabetes: a randomized comparison of chlorpropamide and insulin, Diabetes Care 8 (1985), pp. 219–223.
[36] M.K. Mater, D. Pan, W.G. Bergen and D.B. Jump, Arachidonic acid inhibits lipogenic gene expression in 3T3-L1 adipocytes through a prostanoid pathway, J Lipid Res 39 (1998), pp. 1327–1334.
[37] C. Nugent, J.B. Prins, J.P. Whitehead, J.M. Wentworth, V.K. Chatterjee and S. O'Rahilly, Arachidonic acid stimulates glucose uptake in 3T3-L1 adipocytes by increasing GLUT1 and GLUT4 levels at the plasma membrane. Evidence for involvement of lipoxygenase metabolites and peroxisome proliferator-activated receptor gamma, J Biolumin Chemilumin 276 (2001), pp. 9149–9157.
[38] C.C. Chen, C.Y. Hsiang, A.N. Chiang, H.Y. Lo and C.I. Li, Peroxisome proliferator-activated receptor gamma transactivation-mediated potentiation of glucose uptake by Bai-Hu-Tang, J Ethnopharmacol 118 (2008), pp. 46–50.
[39] D.C. Lagace and M.W. Nachtigal, Inhibition of histone deacetylase activity by valproic acid blocks adipogenesis, J Biolumin Chemilumin 279 (2004), pp. 18851–18860.
[40] D.C. Lagace, R.S. McLeod and M.W. Nachtigal, Valproic acid inhibits leptin secretion and reduces leptin messenger ribonucleic acid levels in adipocytes, Endocrinology 145 (2004), pp. 5493–5503.
[41] Y. Suzuki, K. Kondo, Y. Ikeda and K. Umemura, Antithrombotic effect of geniposide and

genipin in the mouse thrombosis model, Planta Med 67 (2001), pp. 807–810.
[42] C.Y. Zhang, L.E. Parton, C.P. Ye, S. Krauss, R. Shen and C.T. Lin et al., Genipin inhibits UCP2-mediated proton leak and acutely reverses obesity- and high glucose-induced beta cell dysfunction in isolated pancreatic islets, Cell Metab 3 (2006), pp. 417–427.